Effect of Lithium Addition in 8090 Aluminium Alloy on Strengthening Mechanisms and Wear Behaviour of New Generation Aerospace Alumina Nanoparticle Metal Matrix Composites

A CHENNAKESAVA REDDY
PROFESSOR, DEPARTMENT OF MECHANICAL ENGINEERING, JNT UNIVERSITY, HYDERABAD TELANGANA, INDIA
E-mail: chennakesava@jntuh.ac.in

Abstract

Very recently the use of 8090 Al alloy has tremendously increased in the automotive and aerospace industries. This work was focused to understand the effect of lithium content in 8090 Al alloy on the enhancement of tensile, elastic modulus and wear resistance of alumina/8090 Al alloy composites cast by stir casting route. The strength, stiffness and wear resistance were improved due to increase in wettability. The other mechanisms, which could boost properties of alumina/8090 Al alloy composites, were grain boundary strengthening, sub-grain strengthening, nanoparticle strengthening, precipitation strengthening and quench strengthening.

Keywords

8090 Al alloy, Lithium, Alumina, Strengthening mechanism, Wear rate, Coefficient of friction.

Introduction

Nanoparticles reinforced metal matrix composites are widely used for aerospace and automotive applications [1]. If the composite is made of alumina nanoparticles as the reinforcement and aluminium as the matrix, the alumina nanoparticles are inclined to form clusters[2-4].The main difficulty encountered in forming alumina-aluminium composites is that molten aluminium does not readily wet alumina. Consequently, the composite consists of nonuniform microstructure, which attributes the reduction in strength, stiffness and wear resistance of the composite[5, 6]. Several aluminium alloys such as 1xxx[7], 2xxx[8], 3xxx[9], 6xxx[10,11] and 7xxx[12] series of Al-alloys have been reinforced with alumina nanoparticles to estimate the strength, stiffness and wear resistance of the respective composites. Surface coating of the reinforcement was adopted to improve interfacial wettability[13, 14]. But the coating methods are applied on fibres and whiskers. Hard ceramic particles (e.g. SiO_2, Al_2O_3, B_4C, Si_3N_4, BN) and soft lubricants (e.g. graphite) have been used to enhance the wear resistance of the Al-alloy matrix[15-19]. The 8xxx series of Al-alloy has not been combined with alumina nanoparticles till date. Lithium (Li) in alloy 8090 delivers exceptionally high strength and modulus, and so this alloy is used for aerospace applications[20]. Addition of lithium to aluminium assists in reducing density and increase in stiffness. High strength is achieved through good load transfer from the matrix to the particulates

and it requires strong bonding at the interface.

The wetting of the alumina (Al_2O_3) nanoparticles by molten aluminium (Al) alloy is critical to the formation of useful metal matrix composites. To secure this, lithium alloying of aluminium has been anticipated to increase the wetting of the alloy on the alumina nanoparticles.

The present investigation aims at fabrication of alumina/8090 Al alloy composites and to assess the enhancement of strength, stiffness and wear resistance for increasing the wettability of alumina nanoparticles by molten 8090 Al alloy.

Materials and Methods

The composite, with 30 vol% alumina content, was produced by the stir casting and low-pressure die-casting process. The matrix was a 8090 aluminium alloy and the chemical composition with varying content of Lithium (Li) is given in Table-1. The reinforcement phases were alumina nanoparticles with average size of 100 nm.The cast composites were given T3 heat treatment. The flat-rectangular tensile specimen used in the work is shown in Fig 1. Tensile tests were conducted on a universal testing machine with across load speed of 0.5 mm/min at room temperature (ASTM D3039. A strain gauge was used to determine elongation. The heat-treated samples were also machined to get cylindrical specimens of 6 mm diameter and 30 mm length for the wear tests. A pin-on-disc type friction and wear monitor (ASTM G99) was employed to evaluate the friction and wear behaviour of Al_2O_3/8090 Al alloy composites against hardened ground steel (En32) disc. Knoop microhardness was conducted before and after wear tests of composite samples. Wear surfaces of the test samples were analysed with a scanning electron microscope (SEM) using S-3000N Toshiba SEM. A schematic of pin-on-disc tribometer is shown in Fig 2.

Results and Discussion

Table-1: Chemical composition of 8090 Al alloy

Al	Cr	Cu	Fe	Li	Mg	Mn	Si	Ti	Zn	Zr
94.35 %	0.10%	1.2%	0.25%	2.2 -3.0%	0.90%	0.10%	0.20%	0.10%	0.22%	0.08%

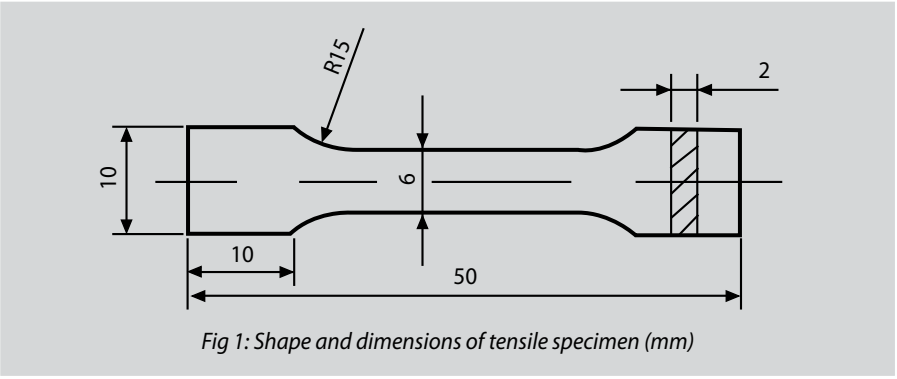

Fig 1: Shape and dimensions of tensile specimen (mm)

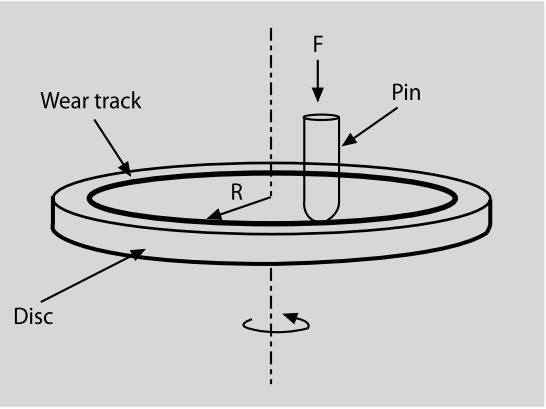

Fig 2: Schematic of pin-on-disc tribometer

The quality of adhesion at the interface is essential for the behaviour of particulate reinforced composites.

Theories for Composite Strength

The adhesive strength at the interface determines the load transfer from the matrix to the particulate. Different approaches were applied to evaluate adhesion between matrix and particulate. As shown in Fig 3, the tensile strength increases with increase in content of Li in 8090 Al alloy which was used to fabricate Al_2O_3/8090 Al alloy composites. The Rule of Mixtures (ROM) is used to predict various properties of a composite material made up of continuous and unidirectional fibres[21]. The ROM is not suitable to predict the strength of discontinuous fibre or particulate metal matrix composites. This is because, in discontinuous metal matrix composites, the ends of each short fibre transfer lesser load than the remainder of the fibre. Hence, other models are required to predict strength and stiffness of particulate metal matrix composites. With some adhesion between the particle and the matrix, the strength of the composite is given by Lu et al [22]:

$\sigma_c = \sigma_m (1-1.07v_p^{2/3})$.....(1)

This expression is inadequate as the experimental strength of the composite is much higher than that obtained in Eq (1). This expression

imparts low strength to the composite, even though, the tensile strength of the matrix is high owing to insufficient adhesive mechanism between nanoparticle and matrix in Eq (1).
An empirical linear relationship

$$\sigma_c = \left[\frac{1-v_p}{1+2.5v_p}\,\sigma_m\right] \exp(Bv_p) \quad \text{.....(3)}$$

where B is an empirical constant, which depends on the surface area of particles, particle density and interfacial bonding energy. For poor interfacial bonding, the particles do not carry any load, so B = 0. As shown in Fig 4, the composites strengths were predicted for the range of B varying from 3.0 to 3.5. For B =3.4, the composite strength was nearly equal to the experimental value.
Hojo et al[25] found that the strength of the composite decreased with increasing mean particle size dp according to the relation:

$$\sigma_c = \sigma_m + k(v_p)d_p^{-1/2} \quad \text{.....(4)}$$

where $k_p(v_p)$ is a constant being a function of the particle loading; k_p is relative change in strength of matrix due to the presence of the particulate. The values of k_p are 0.37, 0.48 and 0.56, respectively, for the Li concentrations of 2.2, 2.6 and 3.0 vol% in aluminium as obtained from tensile strength plots. Even though, the results coincide with the test results, this model does not consider the voids/porosity formation during stir casting of the composites.
A new criterion[26,27] has been formulated considering adhesion, formation of precipitates, particle size, agglomeration, voids/porosity, obstacles to the dislocation, and the interfacial reaction of the particle/ matrix. The formula for the strength of composite is given below:

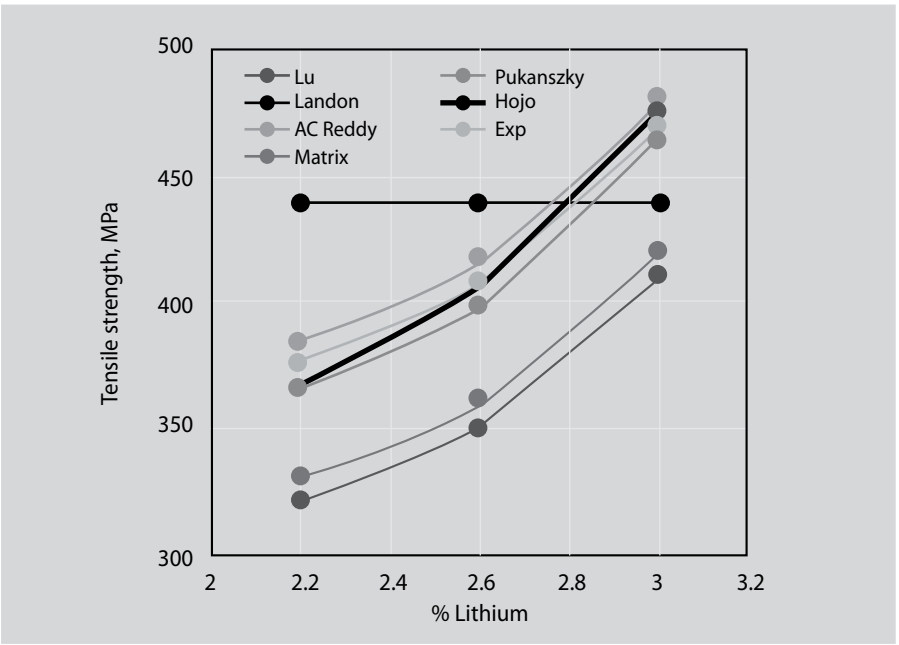

Fig 3: Tensile strength of Al_2O_3/8090 Al alloy composites as a function of lithium concentration

between composite strength and particle size was anticipated by Landon et al [23], which is given by:

$$\sigma_c = \sigma_m (1-v_p) - k(v_p)d_p \quad \text{.....(2)}$$

where $k(v_p)$ is the slope of the tensile strength against the mean particle size and is a function of particle volume fraction v_p. As seen from Fig 3, the strength values were unchanged for the change in the composition of 8090 Al alloy. This expression does not reflect the alloying effect of lithium in aluminium. Equation (2) is applicable to poorly bonded micro-particles but cannot be applied to strong interfacial adhesion, especially for nanocomposites.
For very strong particle-matrix interfacial bonding, Pukanszky et al[24] gave an empirical relationship as mentioned below:

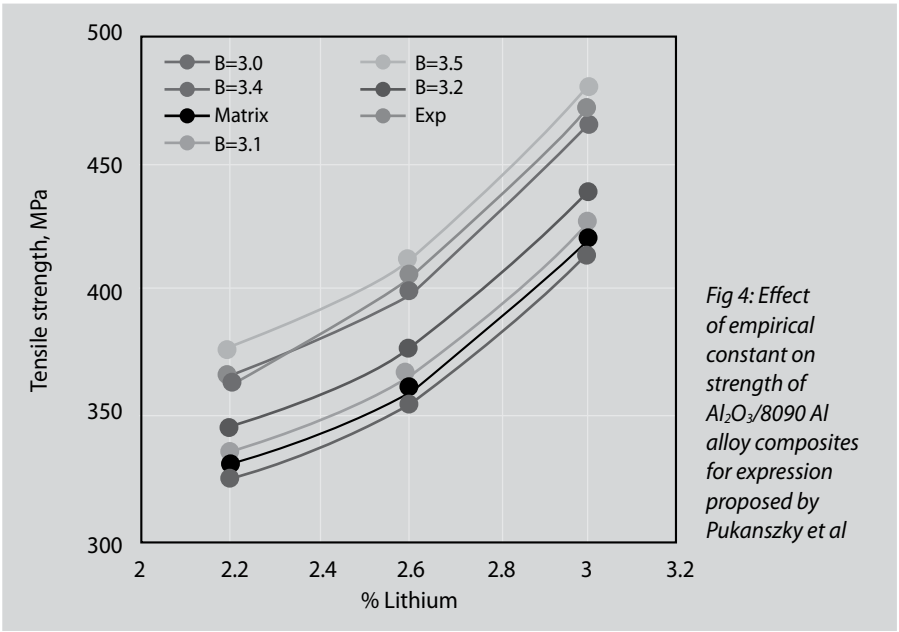

Fig 4: Effect of empirical constant on strength of Al_2O_3/8090 Al alloy composites for expression proposed by Pukanszky et al

$$\sigma_c = \left[\sigma_m \left\{ \frac{1-(v_p-v_v)^{2/3}}{1-1.5(v_p-v_v)} \right\} e^{m_p(v_p-v_v)} + k d_p^{-1/2} \right] \quad \text{..... (5)}$$

$k = E_m m_m / E_p m_p$

where v_v and v_p are the volume fractions of voids and the nanoparticle in the composite, m_m and m_p are the Poisson's ratios of the matrix and nanoparticles and d_p is the mean diameter of the nanoparticle. The results obtained from the model considering voids in the composites[26, 27] were nearly equal to the experimental values.

The models proposed by Lu et al[22] and Landon et al[23] did not take into account microstructural changes in the matrix due to loading of nanoparticles. The microstructures of Al_2O_3/8090 Al alloy composites are shown in Fig 5. The strengthening mechanisms include: grain boundary strengthening (Hall-Petch strengthening), sub-grain strengthening, nanoparticle strengthening, precipitation strengthening and quench strengthening.

A grain boundary can obstruct the dislocation motion in two ways: (1) by forcing the dislocation to change its direction of motion (Fig 6a) and (2) discontinuity of slip plane because of disorder (Fig 6b). Effectiveness of grain boundary depends on its characteristic misalignment, represented by an angle. This angle is higher than 5 degrees in 8090 Al alloy (matrix) in Al_2O_3/8090 Al alloy composites. Since, the lattice structure of adjacent grains differs in orientation, it requires more energy for a dislocation to change directions and move into the adjacent grain. Arsenault and Fisher[28] proposed the enhanced strength observed in Al/SiC composites could be accounted for by a high dislocation density in the aluminium matrix. This high dislocation density was considered to be as a result of large difference (10:1) between aluminium and SiC. Hall-Petch strengthening is limited by the size of dislocations. Once the grain size reaches about 10 nm, grain boundaries start to slide (Fig 7). Also, the T3 heat treatment changes the recrystallisation process leading to grain size modification. Decreasing grain size decreases the number of dislocations at the boundary, increasing the amount of applied

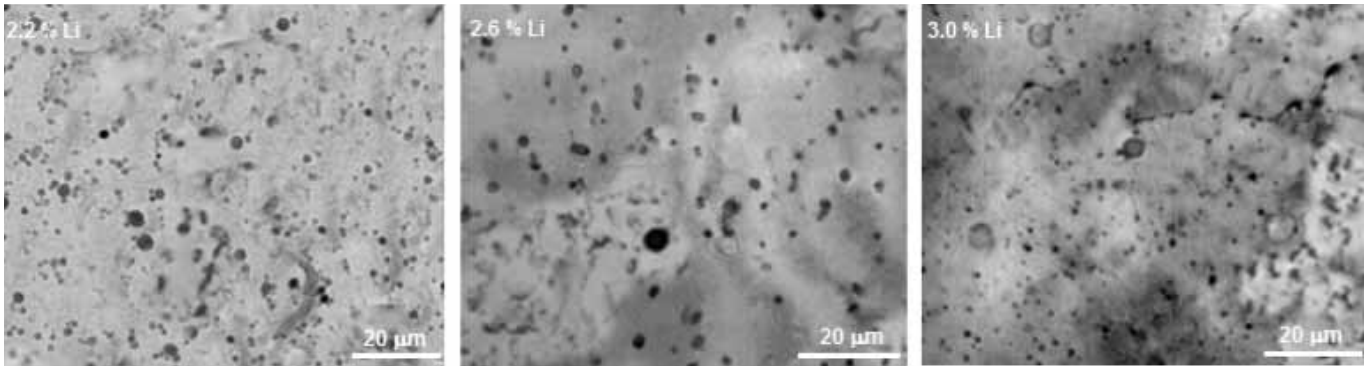

Fig 5: Microstructures of Al_2O_3/8090 Al alloy composites

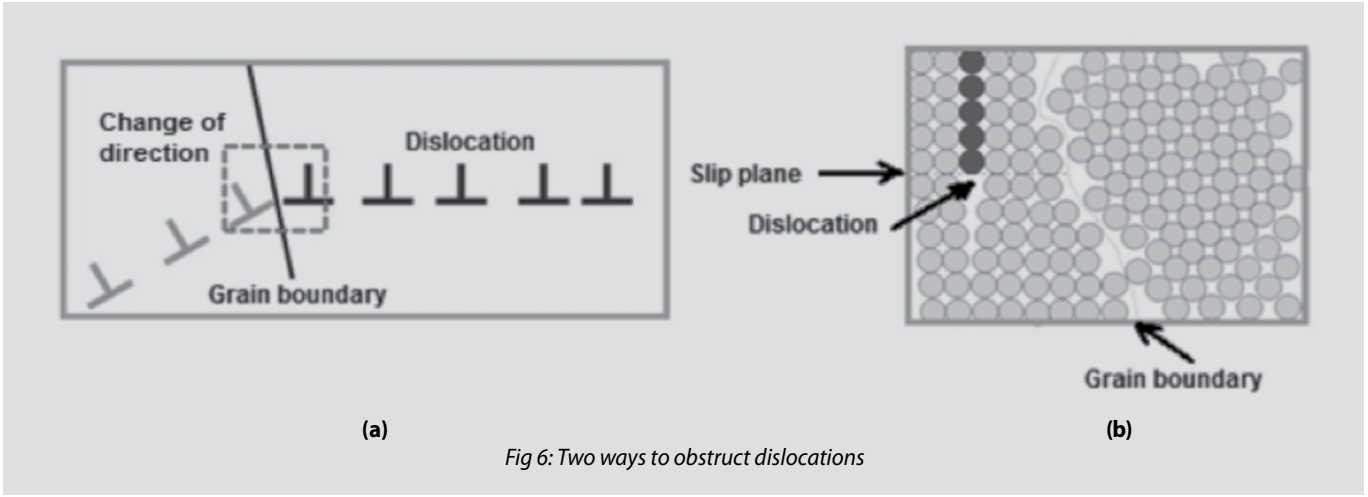

Fig 6: Two ways to obstruct dislocations

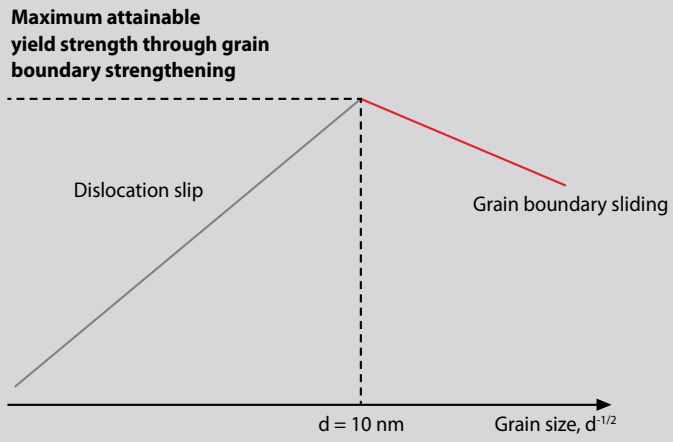

Fig 7: Hall-Petch strengthening

stress necessary to move a dislocation across a grain boundary[29]. The higher the applied stress needed to move the dislocation, the higher the tensile strength. Sub-grain strengthening is owing to sub-grain within the grain that is slightly disoriented from other parts of the grain. When the dislocations accumulate progressively at the grain boundary, the stress concentration takes place at the tip of the leading dislocation resulting in the formation of sub-grain boundary in the 8090 Al alloy as shown in Fig 8. In the nanoparticulate metal matrix composites, the hard nanoparticles are loaded within the matrix. The reinforced nanoparticles would have very little solubility in the matrix[30]. Because of little solubility, the nanoparticles resist growth of grains during the solidification process. The degree of nanoparticle strengthening depends on nanoparticle distribution in the matrix, nanoparticle shape, volume fraction, average particle diameter and mean interspacing of particles. The interspacing of nanoparticles is given by:

$$\lambda = \frac{4(1-v_p)r}{3p} \quad \text{.....(6)}$$

Smaller the nanoparticles, dislocations can cut through them at lower stresses. On the other hand, larger the particles, the dislocations are distributed at wider distances. The clustering allows the nanoparticles to coalesce into larger and fewer particles. The interspacing is increased causing a decrease in the tensile strength (Fig 9). As the volume fraction of alumina increased in 8090 Al alloy (matrix), the clustering tendency increased leading to the formation of alumina nanoparticle clusters. The interspacing was smaller with smaller clusters than that with bigger clusters. Hence, the reduction load transfer from the matrix to the alumina nanoparticles. The other reason for nanoparticle-strengthened composites, containing 10-100 nm particles, the matrix bears the major

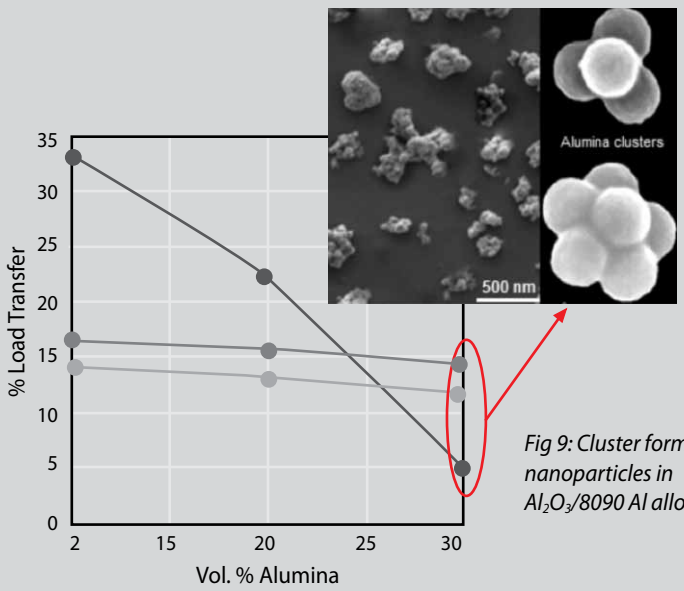

Fig 9: Cluster formation of nanoparticles in Al_2O_3/8090 Al alloy composites

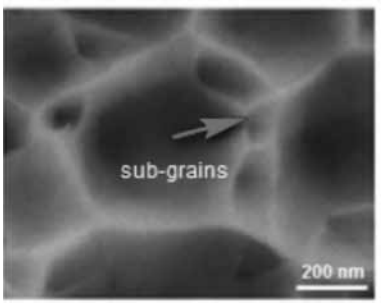

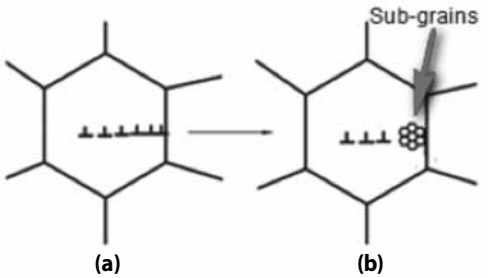

Fig 8: Formation of sub-grains in 8090 Al alloy

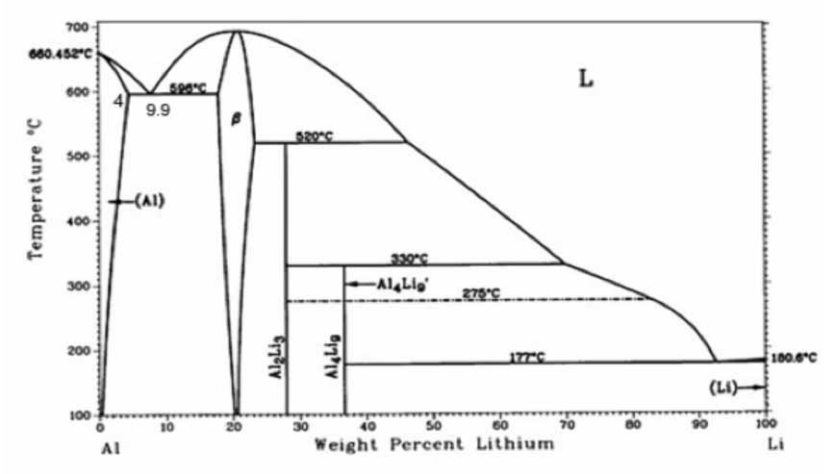

Fig 10: Al-Li phase diagram

Al_4Li, Al_2Li_3, AlLi and $Al_{53}Mg_{14}Li_{33}$. From the Al-Li-Cu ternary phase diagram (Fig 12), the anticipated strengthening precipitates could be Al_4Li_3, Al_2Li_3, AlLi, Al_2CuLi, $Al_{15}Cu_3Li_2$. Figure 13(a) reveals the formation of strengthening precipitates in 8090 Al alloy. The δ and T_2 phases were present in the three examined samples. θ phases were detected in 8090 Al alloy (Fig 13b) consisting of 0.26% Li. Peaks associated with θ, S', Ω and T_1 phases were found in 8090 Al alloy consisting of 0.30% Li. The precipitation of these phases additionally reduces the contribution

portion of the applied load and the small particles hinder dislocation motion, limiting plastic deformation. As shown in Al-Li phase diagram (Fig 10), the maximum solubility of Lithium in Al is 4%. The strengthening precipitates could be α, β (AlLi), γ (Al_2Li_3)and Al_4Li_9 phases. As 8090 Al alloy consists of considerable amount of Mg and Cu, there is a possibility of Al-Li-Mg and Al-Li-Cu ternary phase diagrams. From the Al-Li-Mg ternary phase diagram (Fig 11), the expected strengthening precipitates could be

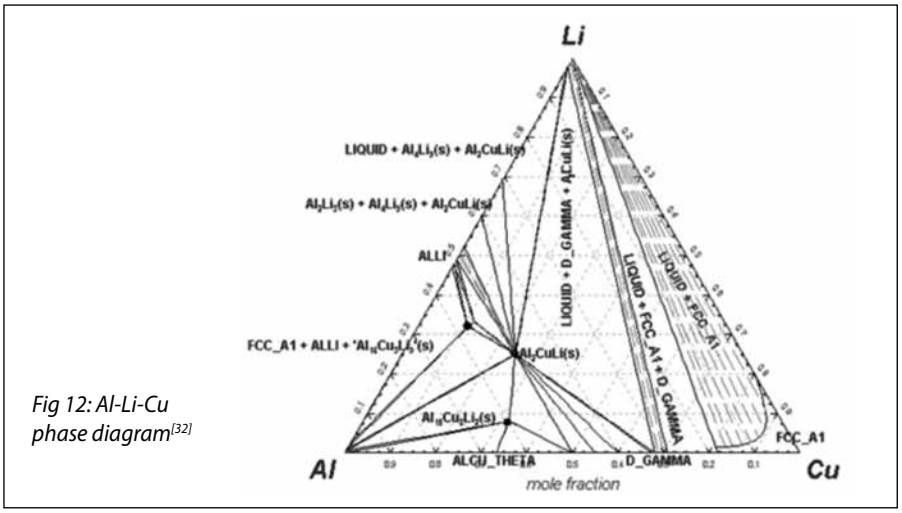

Fig 12: Al-Li-Cu phase diagram[32]

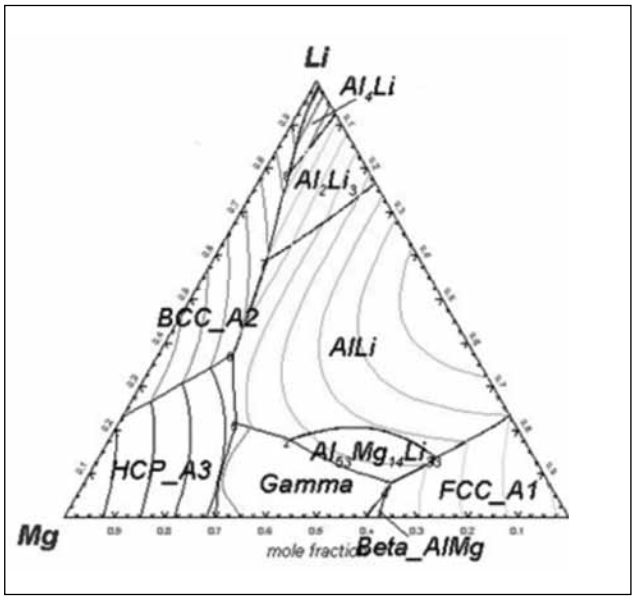

Fig 11: Al-Li-Mg phase diagram[32]

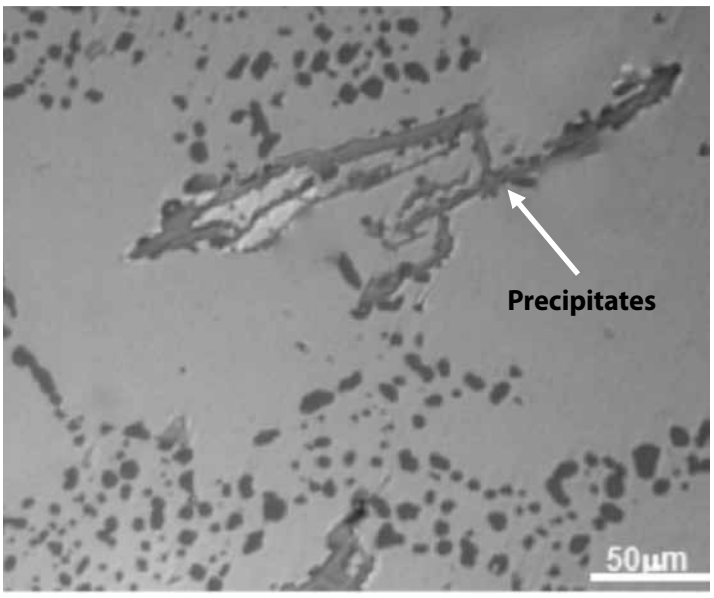

Fig 13(a): Formation of precipitates in 8090 Al alloy (matrix)

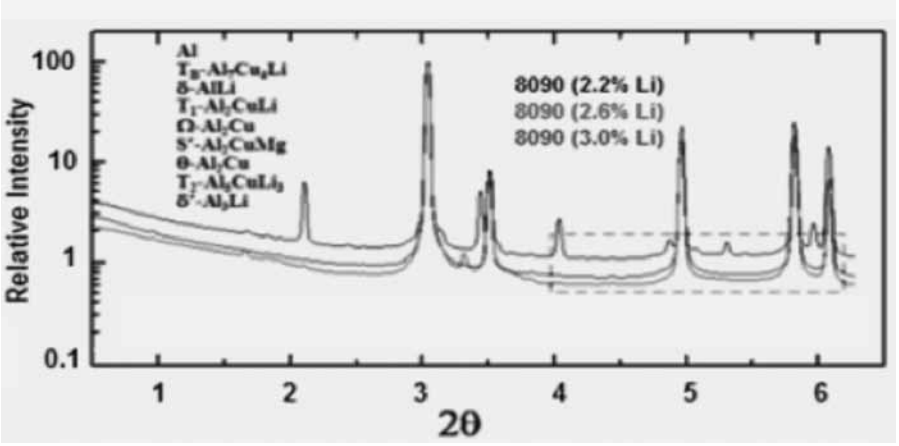

Fig 13(b): EDS analysis of 8090 Al alloys used for Matrix of Al_2O_3/8090 Al alloy composites

of δ phase to strengthening. The coherent strain fields around the strengthening precipitate cause repulsive forces against the dislocation[31]. When the precipitate is coherent and coplanar with the matrix, dislocations in the matrix can readily traverse through the precipitate particles, and if the precipitate and matrix have different structures, then the dislocations which traverse the precipitate create stacking faults in the precipitate. This increase in hardness and strength can be attributed to precipitate strengthening.

Theories for Composite Stiffness

The stiffness of a particulate metal matrix composite is normally determined by the elastic modulus of its components (particle and matrix). Many empirical or semi-empirical equations have been proposed to forecast the modulus of particulate metal matrix composites. Einstein's equation[33] predicts stiffness of particulate composites based on the rigid particle assumption as follows:

$$\frac{E_c}{E_m} = 1+2.5v_p \quad \text{..... (7)}$$

where E_c and E_m are elastic modulus of composite and matrix, and V_p is nanoparticle volume fraction. Einstein's equation for elastic modulus of particulate composites is valid only at low concentrations of reinforcement and assumes perfect adhesion between reinforcement and matrix and uniform dispersion of reinforced nanoparticles[34]. In the present work, the volume fraction of Al_2O_3 nanoparticles was 30 vol%. Hence, the estimated elastic modulus was not correct representative of Al_2O_3/8090 Al alloy composites (Fig 14a). Another equation to estimate the stiffness of a composite that contains spherical particles in a matrix is due to Kerner[35] and it is given below:

$$\frac{E_c}{E_m} = 1+ \frac{v_p}{(1-v_p)} X \frac{15(1-v_m)}{(8-10v_m)} \quad \text{..... (8)}$$

This equation is valid for microparticles of reinforcement. The present work dealt with alumina nanoparticles. Counto[36] proposed a simple model for a two-phase particulate composite by assuming perfect bonding between filler and matrix. The composite modulus is given by

$$\frac{1}{E_c} = \frac{1-v_p^{1/2}}{E_m} + \frac{1}{(1-v_p^{1/2})/ v_p^{1/2} E_m + E_p} \quad \text{..... (9)}$$

This equation did not consider the formation of voids during the fabrication of composites by stir casting technique. Ishai and Cohen[37] assumed that the two constituents are in a state of macroscopically homogeneous stress and adhesive bonding is perfect at the interface between particulate and matrix. When a uniform stress is applied on the boundary, the elastic modulus of the particulate composite is given by

$$\frac{E_c}{E_m} = 1+ \frac{1+(\delta-1)\, v_p^{2/3}}{1+(\delta-1)\,(v_p^{2/3}-v_p)} \quad \text{..... (10)}$$

$$\frac{E_c}{E_m} = 1+ \frac{v_p}{\delta/(\delta-1)\,-v_p^{1/3}} \quad \text{..... (11)}$$

$\delta=E_p/E_m$

Equation (10) and Eq. (11) are for upper-bound and lower-bound solutions. The Rule of Mixtures (ROM) can also be used to predict the elastic modulus of particulate composites.

Upper- bound elastic modulus,

$E_c=v_m E_m+v_pE_p$ ..... (12)

Lower-bound elastic modulus,

$$E_c = \frac{1}{v_m/ E_m + v_p/ E_p} \quad \text{..... (13)}$$

The ROM is valid for continuous fibre-reinforced composites; while the reinforcement was nanoparticles in this work. Hence, the results could not reflect the experimental data. The equations[26,27] to find elastic modulus of composites including perfect boding, interphase between the particle and matrix and the effect of voids/porosity are given below:

$$\frac{E_c}{E_m} = \frac{1-v_p^{2/3}}{1-v_p^{2/3}+ v_p} + \frac{1+(\delta-1)\, v_p^{2/3}}{1+(\delta-1)\,(v_p^{2/3}-v_p)} \quad \text{..... (14)}$$

$$\frac{E_c}{E_m} = 1+ \frac{v_p - v_v}{\delta / (\delta-1) - (v_p+v_v)^{1/3}} \quad \text{..... (15)}$$

$\delta=E_p/E_m$

The Eq. (14) and Eq. (15) represent, the upper limit and lower limit of elastic modulus respectively. The predicted values using Eq. (14) are matching with the experimental data as shown in Fig 14a.

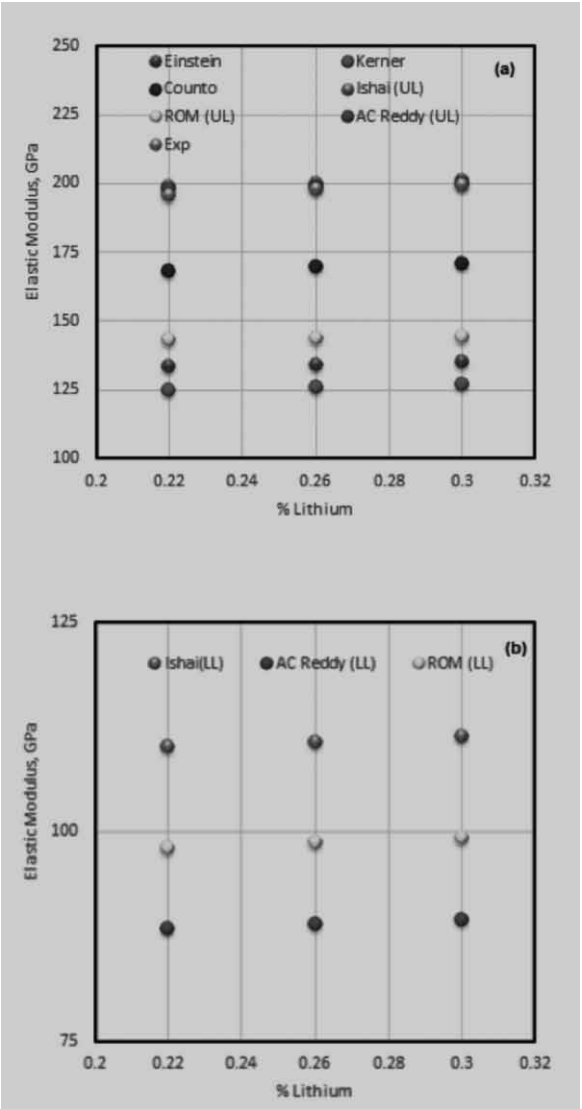

Fig 14: Elastic modulus of Al2O3/8090 Al alloy composites as a function of lithium concentration: (a) upper limit and (b) lower limit

As seen from Fig 14a, Ishai and Cohen model and AC Reddy's model could predict nearly equal elastic modulus (upper limit) of Al_2O_3/8090 Al alloy composites. These models consider perfect bonding between alumina nanoparticles and 8090 Al alloy (matrix). Einstein, Kerner models did not consider the adhesive bonding between the nanoparticle and the matrix. Counto model gave intermediate elastic modulus data on account of poor interface bonding. Ishai and Cohen model gave higher value for the lower limit of elastic modulus than that obtained by AC Reddy's model (Fig 14b). The lower limit of elastic modulus obtained by the rule of mixtures (ROM) is intermediate to that computed by AC Reddy model and Ishai and Cohen model. Every 1% by weight of lithium added to aluminium reduces the density of the resulting alloy by 3% and increases the stiffness by 5%.

Wear Behaviour

Figure 15a shows the dry sliding wear results obtained by conducting pin-on-disc tribometer. The wear test was conducted at a sliding velocity of 1.5 m/s, normal force of 30 N and sliding distance of 1000 m. Owing to the enhancement of wettability by lithium in 8090 Al alloy with the Al_2O_3 nanoparticles, the wear rate decreased with an increase in adhesive bonding between Al_2O_3 nanoparticles and 8090 Al matrix alloy. The influence of lithium content in 8090 on the coefficient of friction of Al_2O_3/8090 Al alloy is shown in Fig 15b. Friction is the value of energy which is dissipated at the material contact surface. Adhesion and deformation are measured the source of frictional forces[38].With increase of lithium in 8090 Al alloy, the coefficient of friction was increased due to number of craters formed on the worn surfaces of Al_2O_3/8090 Al alloy composites. The tendency of crater formation increased with an increase in the content of lithium.

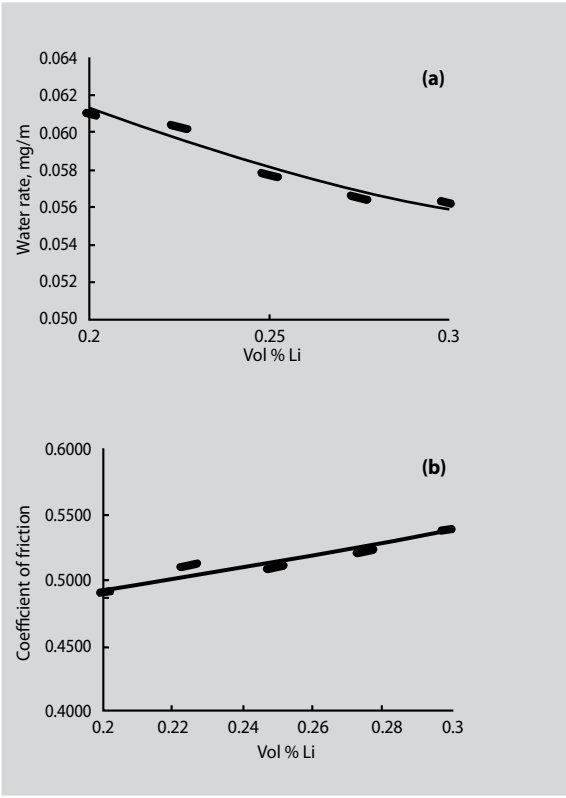

Fig 15: Wear properties of Al_2O_3/8090 Al alloy composites as a function of lithium: (a) wear rate and (b) coefficient of friction

For all the cases, the wear surfaces were nearly alike as shown in Fig 16. Development of craters were detected on the worn surfaces, demonstrating the deformation and delamination of the surface material. In the early stage of wear, nanoparticles are bred from the contact surfaces due to the rubbing possessions of the asperities[39-40]. Some refined particles are dislodged from the composites

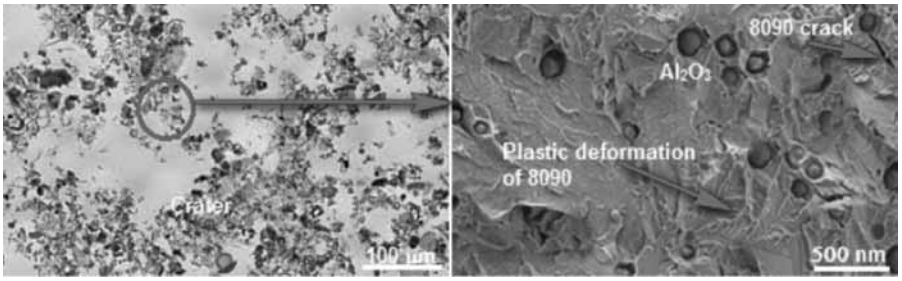

Fig 16: Worn surfaces of AAl2O3/8090 Al alloy composites

whereas some nanoparticle clusters stack at spaces. Since, the nanoparticles have been embedded in very fine-sized debris, the 8090 Al alloy components especially the aluminium and magnesium can be oxidised quickly. Due to the good wettability between 8090 Al alloy and Al_2O_3, the Al-Al_2O_3 interfaces are not the preferential places for the initiation and growth of subsurface cracks. The hardness values of the composites were unchanged with increase of lithium in 8090 Al alloy (Fig 17). A narrow increase in hardness was observed after wear test due to work hardening of the composites.

Conclusions

Every 1% by weight of lithium added to aluminium reduces the density of the resulting alloy by 3% and increases the stiffness by 5%. Its use is aimed at applications where damage tolerance and the lowest possible density are critical.The higher the applied stress needed to move the dislocation, the higher is the tensile strength. As the volume fraction of alumina increased in 8090 Al alloy (matrix), the clustering tendency was increased leading to the formation of alumina nanoparticle clusters. The strengthening precipitates could be α, β (AlLi), γ (Al_2Li_3), Al_4Li_9, $Al_{53}Mg_{14}Li_{33}$, Al_2CuLi and $Al_{15}Cu_3Li_2$. Owing to the enhancement of wettability by lithium in 8090 Al alloy with the Al_2O_3 nanoparticles, the wear rate decreased with an increase in adhesive bonding between Al_2O_3 nanoparticles and 8090 Al matrix alloy. A narrow increase in hardness was observed after wear test due to work hardening of the composites.

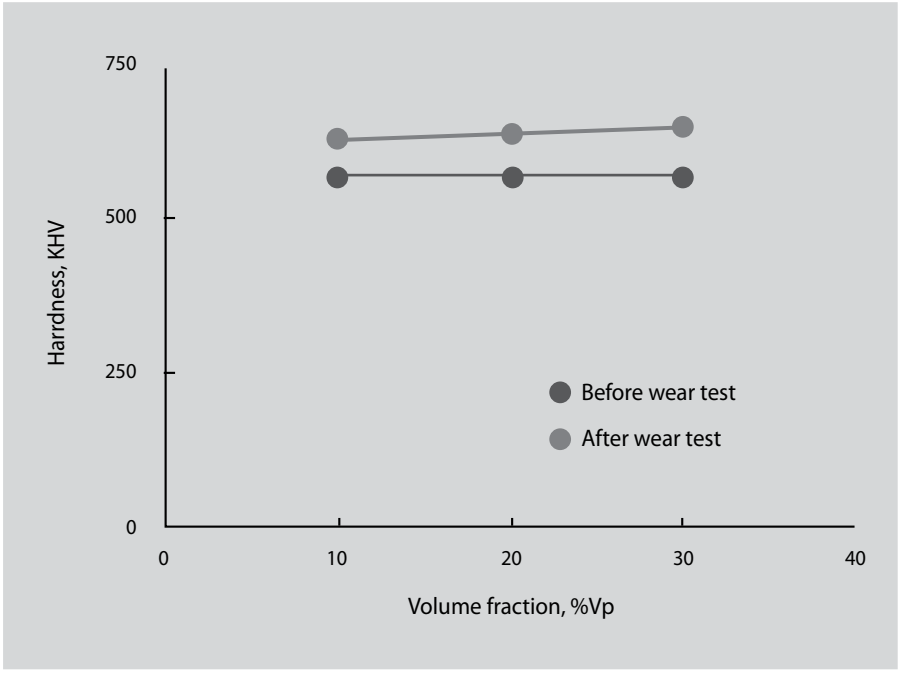

Fig 17: Function of Knoop hardness with volume fraction of CB nanoparticles

Acknowledgement

The authors thanks University Grants Commission (UGC), New Delhi for sponsoring this project.

References

1. A C Reddy, B Kotiveerchari, P Rami Reddy, Saving of Thermal Energy in Air-Gap Insulated Pistons Using Different Composite Materials for Crowns, International Journal of Scientific & Engineering Research, Vol 6, No 3, 2015, p 71-74.
2. A C Reddy, Cause and Catastrophe of Strengthening Mechanisms in 6061/Al_2O_3 Composites Prepared by Stir Casting Process and Validation Using FEA, International Journal of Science and Research, Vol 4, No 2, 2015, p 1272-1281.
3. A C Reddy, Cause and Catastrophe of Strengthening Mechanisms in 6063/Al_2O_3 Composites Prepared by Stir Casting Process: Validation through FEA, International Journal of Scientific & Engineering Research, Vol 6, No 3, 2015, p 75-83.
4. A C Reddy, Cause and Catastrophe of Strengthening Mechanisms in 7020/Al_2O_3 Composites Prepared by Stir Casting Process and Validation through FEA, International Journal of Advanced Research, Vol 3, No 3, 2015, p 603-614.
5. A C Reddy, Essa Zitoun, Matrix Al-alloys for Alumina Particle Reinforced

Metal Matrix Composites, Indian Foundry Journal, Vol 55, No 1, 2009, p 12-16.
6. A C Reddy, Evaluation of Mechanical Behavior of Al-alloy/Al2O3 Metal Matrix Composites with respect to Their Constituents using Taguchi, International Journal of Emerging Technologies and Applications in Engineering Technology and Sciences, Vol 4, No 2, p 26-30, 2011.
7. Y C Kang, S L I Chan, Tensile Properties of Nanometric Al2O3 Particulate Reinforced Aluminium Matrix Composites, Journal of Materials Chemistry and Physics, Vol 85, p 438-443, 2004.
8. J.W. Kaczmar, K. Naplocha, Wear Behaviour of Composite Materials Based on 2024 Al-Alloy Reinforced with Δ Alumina Fibres, Journal of Achievements in Materials and Manufacturing Engineering, Vol 43, No 1, 2010, p 88-93.
9. C. R. Alavala, Prediction Models for Sliding Wear of AA3003/Al2O3 Composites, International Journal of Engineering Research and Application, Vol 6, No 7, 2016, p 20-24.
10. A C Reddy, Essa Zitoun, Tensile Properties and Fracture Behavior of 6061/Al2O3 Metal Matrix Composites Fabricated by Low Pressure Die Casting Process, International Journal of Materials Sciences, Vol 6, No 2, 2011, p147-157.
11. A C Reddy, Essa Zitoun, Tensile Behavior of 6063/Al2O3 Particulate Metal Matrix Composites Fabricated by Investment Casting Process, International Journal of Applied Engineering Research, Vol 1, No 3, 2010, p 542-552.
12. A C Reddy, Strengthening Mechanisms and Fracture Behavior of 7072Al/Al_2O_3 Metal Matrix Composites, International Journal of Engineering Science and Technology, Vol 3, No 7, 2011, p 6090-6100.
13. A Kitahara, S Akiyama, H Uenno, Effects of Alumina Coating on Degradation, Wettability and Bonding Ability of Carbon Fiber with Aluminum, Journal of Japan Institute of Light Metals, Vol 40, No 4, 1990, p 305-311.
14. A C Reddy, Estimation of Thermoelastic Behavior of Three-phase: AA1100/Ni-Coated Boron Carbide Nanoparticle Metal Matrix Composites, International Journal of Scientific & Engineering Research, Vol 6, No 10, 2015, p 662-667.
15. C R Alavala, Nano-mechanical Modeling of Thermoelastic Behavior of AA6061/silicon oxide nanoparticulate metal matrix composites, International Journal of Science and Research, Vol 5, No 1, 2016, p 550-553.
16. C R Alavala, Nanomodeling of Nonlinear Thermoelastic Behavior of AA5454/ Silicon Nitride Nanoparticulate Metal Matrix Composites, International Journal of Engineering Research and Application, Vol 6, No 1, 2016, p 104-109.
17. C R Alavala, Thermoelastic Behavior of Nanoparticulate BN/AA5050 Alloy Metal Matrix Composites, International Journal of Engineering and Advanced Research Technology, Vol 2, No 1, 2016, p 6-8.
18. C R Alavala, Synthesis and Tribological Characterization of Cast AA1100-B4C Composites, International Journal of Science and Research, Vol 5, No 6, 2016, p 2404-2407.
19. A C Reddy, Reduction of Vibration and Noise using AA 7020/Al_2O_3 Nanocomposite Gear Box in Lathe, International Journal of Scientific & Engineering Research, Vol 6, No 9 p 671-677, 2015.
20. S N N Lloyd, M D Patricia, A H David, Interactions between Drops of A Molten Al-Li Alloy with Liquid Water, Metallurgical and Materials Transactions B, Vol 25, No 4, 1994.
21. M S M Alger, Polymer Science Dictionary, Springer Publishing, 2nd Ed, 1997.
22. S Lu, L Yan, X Zhu, Z Qi, Microdamage and Interfacial Adhesion in Glass Bead-Filled High-Density Polyethylene, Journal of Materials Science, Vol 27, 1992, p 4633-4638.
23. G. Landon, G. Lewis, G. Boden, The Influence of Particle Size on the Tensile Strength of Particulate-Filled Polymers, Journal of Materials Science, Vol 12, 1977, p 1605-1613.
24. B. Pukanszky, B. Turcsanyi, F. Tudos, Effect of Interfacial Interaction on the Tensile Yield Stress of Polymer Composites, in: Ishida H, Editor, Interfaces in Polymer, Ceramic and Metal Matrix Composites, Amsterdam: Elsevier; 1988, p 467–477.
25. H Hojo, W Toyoshima, M Tamura, N Kawamura, Short- and Long Term Strength Characteristics of Particulate-filled Cast Epoxy Resin, Polymer Engineering & Science, 1974, Vol 14, p 604-609.
26. A C Reddy, Effects of Adhesive and Interphase Characteristics between Matrix and Reinforced Nanoparticle of AA6061/AlN Nanocomposites, International Journal of Nanotechnology and Application, Vol 5, No 5, 2015, p 1-10.
27. A C Reddy, Effects of Adhesive and Interphase Characteristics between Matrix and Reinforced Nanoparticle of AA2124/AlN Nanocomposites: Mathematical and Experimental Validation, International Journal of Engineering and Advanced Technology, Vol 5, No 1, 2015, p 5-12.
28. R J Arsenault and R M Fisher, Microstructure of Fiber and Particulate SiC in 6061 Al Composites, Scripta Metallurgica, Vol 17, 1983, p 67-71.
29. A C Reddy, Strengthening

Mechanisms and Fracture Behavior of 7072Al/Al_2O_3 Metal Matrix Composites, International Journal of Engineering Science and Technology, Vol 3, No 7, 2011, p 6090-6100.
30. W D Callister, Fundamentals of Materials Science and Engineering, 2nd Ed, Wiley & Sons, p 252.
31. M E Fine, Precipitation Hardening of Aluminium Alloys, Metallurgical and Materials Transactions A, Vol 6, 1975, p 625-637.
32. www.FactSage.com
33. A Einstein, Ueber die von der molekularkinetischen fluessigkeitensuspendierten teilchen, Annals of Physics (Leipzig), Vol 17, 1905, p 549-560.
34. I H Tavman, Thermal and Mechanical Properties of Aluminum Powder-filled High-density Polyethylene Composites, Journal of Applied Polymer Science, Vol 62, 1996, p 2161-2167.
35. E Guth, Theory of Filler Reinforcement, Journal of Applied Polymer Science, Vol16, 1945, p 20-25.
36. U J Counto, Effect of the Elastic Modulus, Creep and Creep Recovery of Concrete, Magazine Concrete Research, Vol 16, 1964, p129-138.
37. O Isha, I J Cohen, Elastic Properties of Filled and Porous Epoxy Composites, International Journal of Mechanical Sciences, Vol 9, 1967, p 539-546.
38. A C Reddy, B Kotiveerachari, Influence of Microstructural Changes Caused by Ageing on Wear Behaviour of Al6061/SiC Composites, Journal of Metallurgy & Materials Science, Vol 53, No 1, p 31-39, 2011.
39. C R Alavala, Tribological Investigation of the Effects of Particle Volume Fraction, Applied Load and Sliding Distance on AA4015/Titania Nanocomposites, IPASJ International Journal of Mechanical Engineering, vol. 4, No. 10, 2016, p 9-15.
40. C R Alavala, Influence of Debris on Wear Rate of Metal Matrix Composites, Journal of Materials Science & Surface Engineering, Vol 4, No 6, 2016, p 458-462.

IFJ Editorial Programme 2017-18

Indian Foundry Journal invites technical papers and articles on topics listed below:

Issue	Focus Subject	Deadlines	
		Editorial	Advertising
October, 2017	Energy Efficiency & Waste Management	September 15, 2017	September 25, 2017
November, 2017	Innovation & New Technologies	October 15, 2017	October 25, 2017
December, 2017	Steel Casting Technology	November 15, 2017	November 25, 2017
January, 2018	Finance & Business Trends	December 15, 2017	December 25, 2017
February, 2018	Process Control	January 15, 2018	January 25, 2018
March, 2018	Plant Engineering & Maintenance	February 15, 2018	February 25, 2018
April, 2018	Marketing & Exports of Castings	March 15, 2018	March 25, 2018
May, 2018	Testing & Measurement	April 15, 2018	April 25, 2018
June, 2018	Clean Foundry, Environment, Health & Safety	May 15, 2018	May 25, 2018